A Generalized Method to Combat Multipaths for RFID Sensing

Ge Wang, Xiaofeng Shi, *Graduate Student Member, IEEE*, Haofan Cai, Chen Qian, *Senior Member, IEEE*, Han Ding, Wei Xi, *Member, IEEE, ACM*, Kun Zhao, *Member, IEEE, ACM*, Jizhong Zhao, *Member, IEEE, ACM*, and Jinsong Han, *Senior Member, IEEE, ACM*

***Abstract*— There have been increasing interests in exploring the sensing capabilities of RFID to enable numerous IoT applications, including object localization, trajectory tracking, and human behavior sensing. However, most existing methods rely on the signal measurement either in a low multipath environment, which is unlikely to exist in many practical situations, or with special devices, which increase the operating cost. This paper investigates the possibility of measuring 'multi-path-free' signal information in multipath-prevalent environments simply using a commodity RFID reader. The proposed solution, Clean Physical Information Extraction (CPIX), is universal, accurate, and compatible to standard protocols and devices. CPIX improves RFID sensing quality with near zero cost – it requires no extra device. We implement CPIX and study three major RFID sensing applications: tag localization, device calibration and human behavior sensing. CPIX reduces the localization error by 30% to 50% and achieves the MOST accurate localization by commodity readers compared to existing work. It also significantly improves the quality of device calibration and human behaviour sensing.**

***Index Terms*— RFID, sensing, multipath, localization.**

Manuscript received 8 April 2020; revised 19 January 2021; accepted 6 July 2022; approved by IEEE/ACM TRANSACTIONS ON NETWORKING Editor M. Li. Date of publication 22 July 2022; date of current version 16 February 2023. This work was supported in part by the National Key Research and Development Program of China under Grant 2018AAA0100500; in part by NSFC under Grant 61832008, Grant 62002284, Grant 61872285, Grant 62072367, and Grant 62032021; in part by the China National Postdoctoral Program for Innovative Talents under Grant BX20200269; in part by the China Postdoctoral Science Foundation under Grant 2020M683494 and Grant 2021M692563; and in part by the Fundamental Research Funds for the Central Universities under Grant xzy012020010 and Grant xzy012020019. The work of Xiaofeng Shi, Haofan Cai, and Chen Qian was supported in part by the National Science Foundation under Grant 1750704, Grant 1932447, and Grant 2114113. *(Corresponding author: Wei Xi.)*

Ge Wang was with the Department of Computer Engineering, University of California at Santa Cruz, Santa Cruz, CA 95064 USA. She is now with the Department of Computer Science and Engineering, Xi'an Jiaotong University, Xi'an 710049, China (e-mail: gewang@mail.xjtu.edu.cn).

Xiaofeng Shi, Haofan Cai, and Chen Qian are with the Department of Computer Engineering, University of California at Santa Cruz, Santa Cruz, CA 95064 USA (e-mail: xshi24@ucsc.edu; hcai10@ucsc.edu; cqian12@ucsc.edu).

Han Ding, Wei Xi, Kun Zhao, and Jizhong Zhao are with the Department of Computer Science and Engineering, Xi'an Jiaotong University, Xi'an 710049, China (e-mail: dinghan@mail.xjtu.edu.cn; xiwei@mail.xjtu.edu.cn; kunzhao@mail.xjtu.edu.cn; zjz@mail.xjtu.edu.cn).

Jinsong Han is with the School of Cyber Science and Technology, Zhejiang University, Hangzhou 310027, China, and also with the Alibaba-Zhejiang University Joint Research Institute of Frontier Technologies, Hangzhou 310007, China (e-mail: hanjinsong@zju.edu.cn).

Digital Object Identifier 10.1109/TNET.2022.3190862

I. INTRODUCTION

AS A COST- and energy-efficient solution for the Internet of Things (IoT), Radio Frequency IDentification (RFID) technology has been widely used to connect tagged objects in ubiquitous applications, such as retailing, warehouse, transportation, and manufactures [1]–[5]. Besides its basic tag-identification function, there has been a growing interest in recent research to discover the sensing capability of RFID tags that reflects the spatial-temporal information of the tags in the physical world [6]–[8]. Typical applications of RFID sensing include localization, trajectory tracking, human behavior sensing, *etc.*. The majority of these applications rely on the measurement of the received signal data from tags, including the *phase shift* between the reader to tags (we use "*phase*" hereafter) and the *received signal strength* (*RSS*).

For example, the phase measurement can help to derive the distance and angle of arrival (AoA) from the reader antennas to a tag and further localize the tag [9], [10]. A successive collection of the phases from a mobile tag can help to determine the moving trajectory of the tagged object [11]–[15]. Phases have also been used for human activity sensing [11], [16]. The RSS can also be used to infer the distance from a tag to the reader or the existence of a moving object around the tag. Hence there have been applications that localize the target tag [17] or detect human gestures [16], [18], [19] by observing the variation of the RSS.

For RFID sensing applications, accurate measurement of *the multipath-free physical information* of the backscatter signals is a must for their correct operations. The multipath-free physical information is defined as the phase and RSS of the signals without environment affection from a tag to the reader, which can reflect the actual distance and relative location changes. In this paper, we call the line-of-sight (LOS) signal phase as the *clean phase* and the RSS that is not affected by the environment as the *clean RSS*. Unfortunately, in most practical RFID setups, signals may be reflected by various reflectors in the environment [17], including walls, furniture, shelves, and moving persons. We consider these environments as *multipath-prevalent* environments. Multiple reflected signals combine with each other and result in measurement results extremely different from the clean ones. We provide an incomplete list of recent research about RFID sensing applications in Table I. We find that they **either cannot combat multipaths or require extra devices/restrictions**. They might assume low-multipath environments, no moving

TABLE I
SOME RECENT RFID SENSING METHODS ("LOCALIZATION" MAY INCLUDE TRAJECTORY TRACKING)

Method	Task	Info. used	Combat multipath	Restrictions
RF-IDraw [11] *SIGCOMM*'14	Localization	Phase	✗	2 readers, 8 antennas, limited space
Tagoram [12] *MobiCom*'14	Localization	Phase	✗	N/A
BackPos [9] *Infocom*'14	Localization	Phase	✗	N/A
STPP [14] *NSDI*'15	Tag ordering	Phase	✗	Mobile antenna
Tagyro [20] *MobiCom*'16	Orientation	Phase	✗	N/A
APID [18] *UbiComp*'16	Behavior sensing	RSS	✗	N/A
RFIPad [21] *ICDCS*'17	Behavior sensing	Phase & RSS	✗	N/A
Tag-Compass [22] *Infocom*'17	Orientation	RSS	✗	N/A
RIO [23]*MobiCom*'17	Behavior sensing	Phase	✗	N/A
ReMix [24]*SIGCOMM*'18	In-body localization	Phase	✗	Non-commodity SDR-based equipments
PinIt [17] *SIGCOMM*'13	Localization	RSS	✓	SDR, mobile antenna, anchor tags
MobiTagbot [25] *MobiSys*'16	Tag ordering	Phase	✓	Mobile antennas, robot, training
BNB [26] *MobiCom*'16	Localization	Phase	✓	Non-commodity devices
RFly [27] *SIGCOMM*'17	Localization	Phase	✓	Drones and Non-commodity devices
RFind [28] *MobiCom*'17	Localization	Phase	✓	Non-commodity SDR-based reader
WiSh [4]*MobiSys*'18	Localization	Phase	✓	Non-commodity SDR-based reader
RF-Echo [29] *MobiCom*'17	Localization	Raw RF signals	✓	Non-commodity tags and reader
TurboTrack [30] *NSDI*'19	Localization	Raw RF signals	✓	Need an SDR-based reader and a complex localization Helper

persons [9], [12], [14], or apply the following two approaches: 1) Collecting plenties of training data in the deployment area to estimate the multipath [13], [15], [25]. This type of methods only considers the static reflectors but obviously does not work when moving persons exist. 2) Using special hardware including Software Defined Radio (SDR) [4], [17], [26]–[30], synchronised antenna array (*e.g.* MUSIC algorithm [31]), moving antennas [17], [25], robots [25], [30], [32], and broadband nonlinear backscatter devices [26]. These methods increase the device cost, may not be compatible with existing RFID systems, and only work for certain specific applications. We specify them in Sec. II.

This paper presents a low-cost, universal, and accurate solution of Clean Physical Information eXtraction (CPIX) in multipath prevalent environments. CPIX **achieves a significant quality gain of RFID sensing with little cost** – it requires no extra device or restriction in addition to the current operating RFID systems: reader, tags, and a data analysis server. Hence it is **a simple yet fundamental improvement** to a diverse group of RFID sensing applications.

We resolve a number of challenges in the design and implementation of CPIX, including the uncontrollable and unpredictable multipath reflections and device diversity. The basic idea of CPIX is to conduct signal measurement from multiple channels of a commodity reader. Our unique innovation is that we decompose the measured data into two parts: the contribution determined by the LOS signal and the contribution by the reflected signals, and then derive their mathematical relationships.

The state-of-the-art RFID systems can benefit from CPIX and obtain a much more accurate phase and signal strength measurement by simply installing the CPIX middleware program at a backend server connected to the reader. We thoroughly evaluate the effectiveness of CPIX by implementing it on three main-stream user applications, namely tag localization, device calibration and human behavior sensing. For tag localization, we utilize the clean phases processed by CPIX as the input of a state-of-the-art hyperbola-based localization method [9]. The CPIX based localization algorithm can achieve median errors of 6.17∼7.63cm (in different setups), which reduce the error of the hyperbola-based localization by 33% to 54% and is **the most accurate tag localization result by commodity devices**. The accuracy is also comparable to or higher than those in low-multipath lab environments by recent methods (some of them only apply to 2D) [9], [12], [14]. We also conduct experiments to evaluate the performance of CPIX in device calibration, a method to reduce data collection errors due to device diversity. The results show that CPIX achieves about 50% error reduction for device calibration. Another implementation is applying CPIX on a recent human behavior recognition application RFIPad [21] and find CPIX improves the accuracy of RFIPad by 10% to 20%. We demonstrate that CPIX is universally applicable to many sensing applications.

Our contributions are summarized as follows.

1) CPIX is the first generalized solution that can measure the multipath-free physical information by only COTS RFID devices. It is a middleware program running on the back server without extra hardware or hardware modification.
2) CPIX needs no deployment of reference/anchor tags or sensors, nor training data collection. It highly improves the application variety and convenience of CPIX.
3) We have done a thorough implementation and validate that CPIX significantly improves the accuracy of tag localization, device calibration and human behavior sensing. We believe CPIX could benefit a diverse group of RFID sensing applications.

The rest of paper is organized as follows. We review the related work in Section II. The model and validation of multipath reflections are presented in Section III. The system design and evaluation can be found in Section IV and V. We discuss current limitations of CPIX in Section VI and VII. Finally we conclude this paper in Section VIII.

II. RELATED WORK

A. Tag Localization and Trajectory Tracking

Due to the close relationship with the travel distance of signals, phases have been widely used in tag trajectory tracking

and localization. BackPos [9] illustrates a specific method for tag localization by constructing a hyperbola with the received phases of the target tags, without using anchor tags. It can achieve a mean accuracy of $12.8cm$ with a variance of $3.8cm$. However, the accuracy of BackPos heavily relies on a low-multipath environment. MobiTagbot [25] is a recent method to determine the orders of a set of tags, which can work in multipath-prevalent environments. It needs extra hardware, i.e., a robot reader with mobile antennas, as well as extra training time. Besides localization, tag trajectory tracking has also been studied [11], [12], [24], [33]–[36]. Tagoram [12] is designed to track a moving tag based on the hologram method using COTS RFID systems. RF-IDraw [11] requires a user to carry a tag on her finger and limit the movement within a small area. Then it can track the detailed trajectory shape of the moving tag with high accuracy. However, the performances of these work also rely on a low-multipath environment. RF-Echo [29], Broadband Nonlinear Backscatter [26], RFind [28] and TurboTrack [30] are recent localization methods that can combat the multipath effect. However, they both require extra hardware such as software-defined radio, non-commodity readers, antenna arrays and even self-defined tags.

B. Human Behavior Sensing

The movement of human body will interference the backscatter communication between the RFID reader and tags. Researchers have studied the relationship between the received phase or signal strength profile and human activities [15], [16], [19], [23], [37]–[42]. Tadar [15] introduces a device-free method for tracking moving objects through a wall. It can remove the influence of static objects, such as furniture, by collecting reference data in advance. RFIPad [21] is a human hand gesture detection system to recognize basic touchscreen operations and English letters. They all rely on low-multipath environments. In recent years, some researchers employ machine-learning tools and algorithms to explore and infer the human behavior among tremendous data in a multipath-prevalent environment. However, it needs considerable hardware costs, including additional antennas and computing support equipments, which limits its applications.

C. LOS Identification Techniques

Prior work in other technologies, such as WiFi and 60GHz wireless, may employ a frequency domain transform method to identify the line-of-sight signals [28]. The basic idea is to transform the frequency domain signals in a certain bandwidth into a time domain. Based on the fact that LOS signal arrives earliest in time, they choose the first peak as the estimation of the LOS signal. However, this method cannot be applied in COTS RFID system. That is because commercial RFID devices transmit RF signals at a certain central frequency and the bandwidth is extremely small (about 4MHz with InpinJ R420). Even though we can transform the frequency domain signals into the time domain, the LOS signal and other reflected signals will superpose with each other and cannot be distinguished. Besides frequency domain transformation, MUSIC is an algorithm used for finding the emitters' locations. Its basic idea is to estimate the direction of multiple arrived signals. However, this method needs a synchronous antenna array and corresponding supporting devices. However, the COTS RFID systems do not support the synchronous antenna array, even if it equipped with an antenna hub.

D. Multi-Channel Based Signal Measurement

The basic idea of CPIX to find out the internal relationship among the measurement of physical information from multiple channels of the reader and then infer the actual value of the clean phase/RSS. Multi-channel based signal measurement has been used in other technologies, such as WiFi, 60GHz wireless, and acoustic signals [43], [44]. Multi-channel based signal measurement has been used in other technologies, such as WiFi, 60GHz wireless, and acoustic signals. For instance, Wang *et al.* propose a phase-based distance measurement approach for acoustic signals in a recent work LLAP. This method can estimate the dynamic vectors introduced by the movement of hands. However, due to the huge differences in transmission speed, frequency, and protocol design between the acoustic-based approaches and RFID system, the method cannot be applied in COTS RFID devices. While Wi-Fi and some similar techniques, *e.g.*, 60G, transmit and receive multiple sub-channels simultaneously, which can be used to estimate the current channel state information and calculate the possible values of phase. However, RFID devices and protocols work differently from other wireless technologies, and hence these methods cannot be applied directly to RFID. Different from the aforementioned techniques, an RFID reader antenna works on one channel at a time and communicates with only one tag. These limitations introduce a lot of unknown variables and increase the difficulty in our phase estimation and calculation.

Compared with aforementioned super-resolution techniques, CPIX does not need any extra hardware and can be applied in COTS RFID systems. In addition, it can work well in a changing environment, where exists uncontrollable moving objects. In the following sections, we will elaborate the background of RFID-based sensing and introduce our design.

III. Background

Before we introduce our method, we first introduce the propagation model of the passive RFID system. A passive RFID tag communicates with the RFID reader by backscattering its electric signals. Since there are prevalent reflectors in the real world, the received signals at the reader's antenna can be expressed as a superposition of the line-of-sight (LOS) signal $\overrightarrow{P_L}$ and the multipath signals $\overrightarrow{P_{M_m}}$, *i.e.* :

$$\begin{aligned} \overrightarrow{P}(\rho,\beta) &= \overrightarrow{P_L}(\rho_L,\theta) + \overrightarrow{P_M}(\rho_M,\alpha), \\ where\ \overrightarrow{P_M} &= \overrightarrow{P_{M_1}} + \overrightarrow{P_{M_2}} + \ldots \overrightarrow{P_{M_m}} + \ldots \end{aligned} \tag{1}$$

where ρ and β are the amplitude and the observed phase of the received signal. Note that we do not analyze each multipath component individually. As shown in Fig. 1(b), no matter how many multipath components coexist, their superposition can be expressed as a single vector. Hence, we consider their combination, *i.e.*, $\overrightarrow{P_M}$, in our model instead.

In Eq. 1, we can only obtain the amplitude ρ[1] and the observed phase β. However, only the line-of-sight phase θ

[1]The amplitude ρ can be estimated by the received signal strength (RSS), *i.e.*, $\rho = 10^{\frac{RSS}{1000}}$ [12].

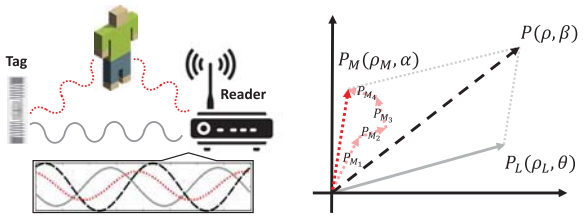

(a) LOS and reflected signal (b) Wave superposition

Fig. 1. RF signal propagation model. The two-dimensional coordinate system in (b) is a polar coordinate system, in which the vectors on this plane represent the RF signals.

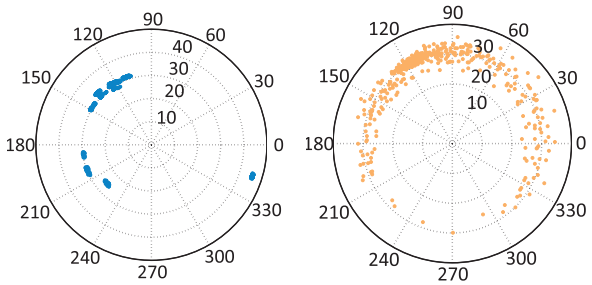

(a) Different environments (b) With mobility

Fig. 2. Phase variations due to multipaths, radian is the phase and radius is the RSS (−dBm).

has the following relationship with the distance between the reader and the tag [9], [12], [15]:

$$\theta = (\theta_A + \theta_T + \theta_D) \mod 2\pi \tag{2}$$

where θ_A and θ_T are the initial phases of the reader antenna and the tag, respectively. And θ_D is the corresponding phase change over the signal travel distance, which is defined as:

$$\theta_D = (2\pi \cdot 2d/\lambda) \mod 2\pi \tag{3}$$

where d is the distance from the antenna to the tag. $\lambda = c/f$ is the wavelength and c is the speed of electromagnetic signal. In contrast, the multipath signal P_M is determined by surrounding reflectors, such as moving objects like human beings, robots and static ones like furniture, walls, *etc.*. In addition, due to the non-negligible reflection attenuation, we have $\rho_M < \rho_L$.

A. Model of Signal Propagation

Observing the aforementioned elaborations, we find that the received signal P is not a linear relationship with the LOS signal P_L. As shown in Fig. 1, the received signal P (black dotted line) is the superposition of the LOS signal P_L (grey line) and current multipath signal P_M (red dotted line). However, we have no information about the multipath signal P_M. As a result, the COTS reader is not able to tell the LOS signal P_L from its received signal P. In other words, the physical data (including phase and RSS) we measured from the received signal cannot accurately reflect the exact values and changes of the LOS signal, causing existing work to be error-prone in multipath-prevalent environments. In the following subsection, we will verify the impact of the multipath effects with experiments.

B. Experimental Analysis of Multipaths

We conduct two sets of experiments using COTS RFID devices to validate that multipath reflections will cause the measurement data (including phase and RSS) from the received signal completely unpredictable and deviated from the LOS ones. The first experiment is to show the ubiquity of multipath in different static environments. We place one tag in front of a reader, and then keep their separation distance unchanged, but move the whole system to 10 different locations in indoor environments. The received phases and RSSs of the same tag are shown in Fig. 2(a),[2] where the radius reflects the absolute value of RSS and the radian shows the degree of phase. We find that the phase measurement results have a huge variance in $(105°, 345°)$. This variance may introduce >20cm errors when calculating the distance ($[\lambda \cdot (345° - 105°)]/360° \approx 21$cm, for $\lambda \approx 32$cm), resulting in a destructive impact on tag localization and trajectory tracking. The second experiment is to investigate the signal fluctuations caused by moving objects. We let the reader keep querying a tag and collecting the signals for 10 seconds. During that time, a volunteer moves around the tag arbitrarily. As shown in Fig. 2(b), the values of phase are widely distributed in the 2π range and the RSS varies in $[-30, -20]$dBm. In other words, the movement of objects around the tag will make the phase and RSS measurements significantly different from the clean physical information and hence damage the performance of RFID sensing applications such as localization, human activity recognition, *etc.*.

[2]Whether the reader works with a fixed frequency or with hopping frequencies do not matter in our design. More details can be found in Sec. VI.

IV. CPIX Design

The objective of CPIX is to extract the clean measurement information, namely the phase and RSS, from a tag in multipath environments. Extracting the multipath-free physical information from the measured data is challenging. **Our unique innovation is that we decompose the measured signals into two parts**: the contribution determined by the LOS signal and the contribution by the reflected signal, and derive their mathematical relationships. We further validate that measurement from different channels can be fitted with a linear function of the two types of contributions, which can be used to extract the clean measurement. CPIX can be separated into three steps, including **1)** Phase decomposition. **2)** Clean phase calculation. **3)** RSS calculation. To be more clear, we list some key parameters used in our algorithm in Table. II.

A. Phase Decomposition

As aforementioned, the received signal is a vector superposition of the LOS signal and other reflected ones. Therefore, in this step, we first explore the relationship between the LOS signal P_L and the received signals P.

We illustrate the relationship between the measured phase β and the clean phase θ, in Fig. 3. The radius of the vector represents the amplitude of the signal and the polar angle represents the current phase. As shown in Fig. 3(a), the gray line $\overrightarrow{OC}$ denotes the line-of-sight signal P_L, while the red

TABLE II
THE KEY PARAMETERS

Para.	Expression	Para.	Expression	Para.	Expression
θ	The phase of the LOS signal.	β, β_n	The received phase (in channel n).	α	The phase of the multipath signals.
$\hat{\theta}$	The mirror-image of θ.	$\hat{\alpha}$, $\hat{\alpha_n}$	The multipath variable (in channel n).	$\Delta\hat{\theta}$	The phase between two adjacent channels.
y'	The ideal line.	κ', d'	The slope and the intercept of the ideal line.	ω_n	The weight of the data in channel n.
y	The fitting line.	κ, d	The slope and the intercept of the fitting line.	y_n	The value on the fitting line at channel n .
φ	The optimization function.	e_1,e_2	The errors introduced by multipath effects.	S_n	The residual error at channel n.

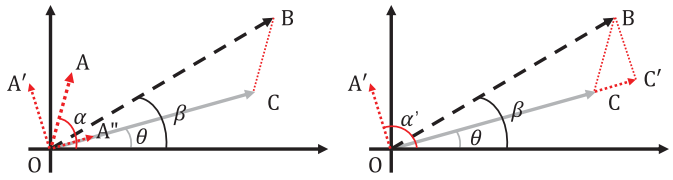

(a) Signals superposition (b) Decompose signals

Fig. 3. Relationships between β and θ.

line $\overrightarrow{OA}$ represents the superposition of all reflected signals, *i.e.*, P_M. Their phases are θ and α, respectively. When $\overrightarrow{OC}$ and $\overrightarrow{OA}$ meet at the receiving antenna, they superpose with each other and form a new signal $\overrightarrow{OB}$, which is reported as the signal measurement, *i.e.*, P.

To extract the relationship between LOS signal $\overrightarrow{OC}$ and the received signal $\overrightarrow{OB}$, we first build a bridge between the multipath signal and LOS signal. As shown in Fig. 3(a), we decompose the multipath vector $\overrightarrow{OA}$ into two parts, one vector $\overrightarrow{OA'}$ is perpendicular to LOS signal $\overrightarrow{OC}$, while another vector $\overrightarrow{OA''}$ is parallel to $\overrightarrow{OC}$. As shown in Fig. 3(b), we let $\overrightarrow{OC'} = \overrightarrow{OC} + \overrightarrow{OA''}$. The new polar angle α' of vector $\overrightarrow{OA'}$ has the following relationship with the former one:

$$\alpha' = (\theta + \frac{\pi}{2} + k_0 \cdot \pi) \ mod \ 2\pi \tag{4}$$

where k_0 is a non-negative integer. Since the reflected signals are completely unknown, the relationship between polar angel α and β are ambiguous too. In the following part, we try to investigate the inner relationship between the superposed phase β' and the two component phases θ' and α'. In the new forms, according to the Phasor arithmetic, we have a following equation:

$$\tan\beta = \frac{|\overrightarrow{OC'}| \cdot \sin\theta + |\overrightarrow{OA'}| \cdot \sin\alpha'}{|\overrightarrow{OC'}| \cdot \cos\theta + |\overrightarrow{OA'}| \cdot \cos\alpha'} \tag{5}$$

Considering the relationship between the values of α' and θ in Eq. 4, if we replace α' with θ in Eq. 5 we have:

$$\tan\beta = \frac{\tan\theta + (-1)^{k_0} \cdot \frac{|\overrightarrow{OA'}|}{|\overrightarrow{OC'}|}}{1 + (-1)^{k_0+1} \cdot \tan\theta \cdot \frac{|\overrightarrow{OA'}|}{|\overrightarrow{OC'}|}} \tag{6}$$

We find that θ and α' do not have a linear relationship with the phase β. In order to process them in a mathematical way, we define two *scalars*, $\hat{\theta}$ and $\hat{\alpha}$, whose sum is the received phase β, *i.e.*,

$$\beta = \hat{\theta} + \hat{\alpha} \tag{7}$$

where $\hat{\theta}$ is the contribution to β determined by θ, and $\hat{\alpha}$ is the contribution to β determined by α. We call $\hat{\theta}$ as the *mirror image phases* of θ and $\hat{\alpha}$ as the *multipath variable*. To explore the internal relationship between the scalars and the real phases, we also calculate the tangent value of β. According to the Trigonometric relation, we have:

$$\tan\beta = \tan(\hat{\theta} + \hat{\alpha}) = \frac{\tan\hat{\theta} + \tan\hat{\alpha}}{1 - \tan\hat{\theta} \cdot \tan\hat{\alpha}} \tag{8}$$

Comparing Eq. 6 and Eq. 8, we find that the two variables, $\hat{\alpha}$ and $\hat{\theta}$, have the following relationship with θ, which will help us to infer the clean phase θ by estimating the value of mirror image phase $\hat{\theta}$:

$$\begin{cases} \hat{\theta} = (\theta + \hat{k} \cdot \pi) \ mod \ 2\pi, where \ \hat{k} \in Z \\ \hat{\alpha} = \arctan((-1)^{k_0} \cdot \frac{|\overrightarrow{OA'}|}{|\overrightarrow{OC'}|}), \end{cases} \tag{9}$$

In this way, we transform the measured phase β from the superposition of two unknown phases into a simple sum of two scalar phases $\hat{\alpha}$ and $\hat{\theta}$. In addition, we build a bridge between the desired clean phase θ and its image phase $\hat{\theta}$ (Eq. 9). In the following section, we will elaborate on how to calculate the value of the image phase $\hat{\theta}$ and finally infer the value of the clean phase θ.

B. Clean Phase Calculation

In the previous section, we find that the measured phase β does not have a linear relationship with the clean phase θ and multipath phase α. Instead, we choose two phases, namely the *multipath variable* $\hat{\alpha}$ and the *mirror image phase* $\hat{\theta}$, and build a linear equation with the measured phase β. In this section, we try to calculate the exact value of the *mirror image phase* $\hat{\theta}$ by exploring the internal relationship among the measured phases β in multiple channels.

To reach this goal, we need to model the measured phase β. We first introduce an observation and our conjecture about the received phase β in multiple channels. Recall that a reader has N channels ($N = 16$ in our experiments). We make a conjecture that the received phase β_n in channel n can be expressed as:

$$\beta_n = \hat{\alpha_n} + \hat{\theta} + (n-1) \cdot \Delta\hat{\theta} \tag{10}$$

where $\hat{\theta}$ refers to the mirror image phase in the first channel. $\hat{\alpha_n}$ is the *multipath variable* in channel n. Note that the

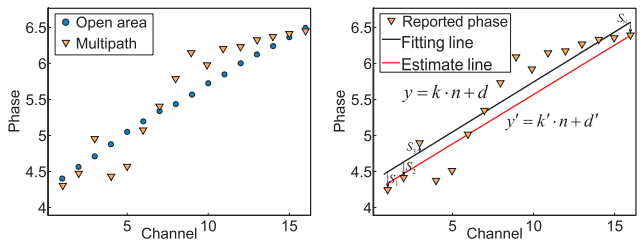

(a) The reported phases (b) The fitting line

Fig. 4. The reported phases in 16 channels.

multipath variables $\hat{\alpha_n}$ in channel n are *different* and *non-linear* for different channels.[3] On the contrary, the phase shift $\Delta\hat{\theta}$ between two adjacent channels is linear. It is composed of three parts, namely the phase changes $\Delta\theta_D$ over distance, phase changes $\Delta\theta_A$ and $\Delta\theta_T$ due to the device characteristics. When the channel is switched from n to $n+1$, the wavelength λ varies. As a result, the received signal over the same distance will incur a phase change of $\Delta\theta_D$. In addition, the initial phases of the antenna and tag will change by $\Delta\theta_A$ and $\Delta\theta_T$, respectively. Here we assume the initial phases $\Delta\theta_A$ and $\Delta\theta_T$ that introduced by the hardware also change linearly. This is reasonable because these phase changes may also be introduced by the wavelength alteration. Observing the three components of $\Delta\hat{\theta}$, we find that all of them are introduced by frequency hopping. As the frequency varies linearly among different channels, the phase shifts $\Delta\hat{\theta}$ should be linear as well.

To validate the aforementioned conjecture, we perform a set of experiments. We place a tag in two different places, *i.e.*, an open area and a multipath-prevalent environment, and record the reported phases β_n in each channel. The results are shown in Fig. 4(a). The measurement phases in the open area are roughly on a straight line y'. That is because the effect of multipath signals in the open area is negligible when it is compared with the line-of-sight one, *i.e.*, $\hat{\alpha_n} \ll \Delta\hat{\theta}$. This assumption is reasonable because the reflections in the open area are much fewer and their propagation paths are much longer. Hence we can safely express the straight line y' as:

$$y' = \kappa' \cdot n + d', where\ \kappa' = \Delta\hat{\theta}, d' = \hat{\theta} - \Delta\hat{\theta} \qquad (11)$$

We call y' as the ideal line, which is only correct when there is no multipath effect. According to Fig. 4(a), the reported phases in the open area (the blue dots) indeed follow the linear relationship, which is consistent with our conjecture. On the other hand, in a narrow space, the multipath effect becomes severe. In the second experiment, the multipath variables $\hat{\alpha_n}$ cannot be ignored. As a result, the phase fluctuates sharply from channel 1 to 16, as outlined by the orange triangles in Fig.4(a).

[3]The reasons are two-fold. First, signals' phases vary with the frequency, which means, even if the reflectors keep stable in the environment, the phases over the same reflection path are also different. Second, the path-loss and reflection attenuation are both different at different transmitting frequencies. The theoretical path loss in free space [45]–[47] is $FSPL(dB) = 20log(d) + 20log(f) - 27.55$. And the reflection attenuation in free space can be denoted as $RL(dB) = 20log\frac{Z_{in}-Z_0}{Z_{in}+Z_0}$, where Z_{in} is the impedance, which is related to the frequency. As a result, the multipath variables $\hat{\alpha_n}$ of different channels will be not only inconformity, but also non-linear.

In fact, the measured data in practice is more likely to be inaccurate and error-prone. To retrieve the exact value of tag's mirror image phase $\hat{\theta}$ from the measured one, *i.e.*, β, we analogize the Eq. 10 as a matrix equation $A \cdot x = b$, *i.e.*,

$$A_{N\times(N+2)} = \begin{bmatrix} 1 & 0 & 0 & \dots & 0 & 1 & 0 \\ 0 & 1 & 0 & \dots & 0 & 1 & 1 \\ 0 & 0 & 1 & \dots & 0 & 1 & 2 \\ \cdot & \cdot & \cdot & \cdot & \cdot & \cdot & \cdot \\ \cdot & \cdot & \cdot & \cdot & \cdot & \cdot & \cdot \\ \cdot & \cdot & \cdot & \cdot & \cdot & \cdot & \cdot \\ 0 & 0 & 0 & \dots & 1 & 1 & N-1 \end{bmatrix},$$

$$x^T_{N+2\times1} = [\hat{\alpha}_1, \hat{\alpha}_2, \hat{\alpha}_3, \dots \hat{\alpha}_N, \hat{\theta}, \Delta\hat{\theta}],$$
$$b^T_{N\times1} = [\beta_1, \beta_2, \beta_3, \dots \beta_N], \qquad (12)$$

where $A_{N\times(N+2)}$ is the coefficients matrix, $x_{(N+2)\times1}$ is the unknown variable matrix, and $b_{N\times1}$ represents the matrix of reported phases. And $(\cdot)^T$ represents the transpose of the matrix. Obviously, Eq. 12 is a set of non-homogeneous linear equations. Since we have $N+2$ unknown variables and N equations, the solution of x has infinite possible candidates. To find out the valid solution of x, we need to establish two more additional equations.

To achieve this goal, we fit these reported phases β_n in all channels into a line. We define the fitting line as $y_n = \kappa \cdot n + d$, which has the minimal φ as follows:

$$\varphi = \sum_{n=1}^{N} \omega_n \cdot (y_n - \beta_n)^2, \qquad (13)$$

where ω_n is the weight of channel n. Intuitively, the multipath effects are not identical for each channel. For some channels, they may be interrupted by unpredictable mobile factors, or just more sensitive than others. We need to evaluate the data quality of each channel and take it into consideration. To reach this goal, we define a weight function to reduce the influence of severe influences of outliers. The principle to determine the weight function is very simple, *i.e.*, a more serious *dynamic* multipath effect leads to more discrete phase reports. As we know, the dynamic reflectors, such as moving objects and humans, will introduce the uncontrollable and unpredictable errors into the measured phases. In contrast, the *static* multipath effect, which introduced by static objects like walls, ceilings, and furniture, will be much more stable and have a normal distribution [2]. Our goal is to reduce the influence of dynamic multipath, and try to estimate the exact effects of static multipath signals. Therefore, we divide the $\hat{\alpha}_n$ into two parts, $\hat{\alpha}_n = \hat{\alpha}^s_n + \hat{\alpha}^d_n$, where $\hat{\alpha}^s_n$ represents the contribution of static reflectors, and $\hat{\alpha}^d_n$ comprises of the impact introduced by moving objects. Compared with the fluctuations introduced by the dynamic factors, the static multipath component $\hat{\alpha}^s_n$ has much lower mean difference (as shown in Fig. 2(a) and 2(b)). We can estimate the data quality by considering the discrete degree of the received phases. Intuitively, the more discrete the received phases are, the more influence that introduces by the uncontrollable dynamic multipath effects. We utilize the sample mean difference σ_n of received phases in channel n to represent the discrete degrees:

$$\sigma_n = \frac{\sum |\beta^0_n - \overline{\beta_n}|}{t}, \qquad (14)$$

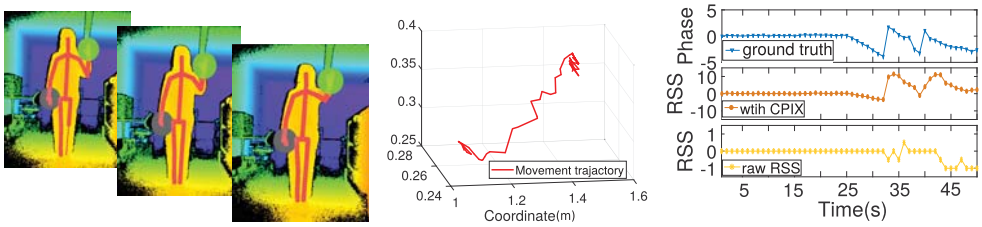

(a) Deapth figure (b) Movement path (c) The profiles of RSS w/o CPIX

Fig. 5. A volunteer pushes the right hand and the ground truth can be obtained by Kinect.

where β_n^0 represents the reported phase samples in channel n, and $\overline{\beta_n}$ is the average value of all the t samples. If there are few dynamic factors, the expectation of σ should be 0. We further define the weight function as:

$$\omega_n = \frac{N \cdot p_n}{\sum p_n}, n = 1, 2, 3 \ldots N, \tag{15}$$

Here we define p_n as follows:

$$p_n = e^{(\sum_{n=1}^{N} \sigma_n) - (N \cdot \sigma_n)} \tag{16}$$

The p_n measures the discrete level of the n-th channel among all the N channels [25]. To make the weighted function easy to solve, we further process the measurement p_n with Eq. 15. The sum of all ω_n equals to the number of channels, *i.e.*, N. In this way, we reduce the weights of severely polluted channels in order to eliminate the impact of the uncontrollable and dynamic multipath effect. Since the dynamic multipath effects follow a Gaussian distribution,[4] when the sample number t is sufficiently large, we can safely make an assumption that:

$$\sum_{n=1}^{N} \omega_n \cdot \hat{\alpha}_n^d \approx 0. \tag{17}$$

The weight function will help us to find a more appropriate fitting line and ultimately, to get accurate results. Note that the weight function only gives a solution to reduce the adverse effects introduced by the dynamic factors, it cannot eliminate the dynamic multipath.

Determining the most appropriate values of rake ratio κ and intercept d for the fitting line requires minimizing φ in Eq. 13. To achieve this goal, we calculate the partial derivative of φ for variable κ and d, respectively:

$$\begin{cases} \frac{\partial \varphi}{\partial \kappa} = \sum_{n=1}^{N} \omega_n \cdot [2n^2\kappa + 2n(d - \beta_n)] \\ \frac{\partial \varphi}{\partial d} = \sum_{n=1}^{N} \omega_n \cdot [2d + 2(\kappa \cdot n - \beta_n)] \end{cases} \tag{18}$$

Let Eq. 18 equals 0 and solve the equations. We have:

$$\begin{cases} \kappa = \Delta\hat{\theta} + e_1, \ e_1 = \frac{N \cdot \sum \omega \cdot n \cdot \hat{\alpha}_n - \sum \omega \cdot n \cdot \sum \omega \cdot \hat{\alpha}_n}{N \cdot \sum \omega \cdot n^2 - (\sum \omega \cdot n)^2} \\ d = \hat{\theta} - \Delta\hat{\theta} + e_2, \ e_2 = \frac{\sum \omega \cdot n^2 \cdot \sum \omega \cdot \hat{\alpha}_n - \sum \omega \cdot n \cdot \hat{\alpha}_n \cdot \sum \omega \cdot n}{N \cdot \sum \omega \cdot n^2 - (\sum \omega \cdot n)^2} \end{cases} \tag{19}$$

We find that the slope κ and the intercept d of the fitting line y have an error e_1 and e_2 with that of the ideal line, respectively. If we can make sure the value of the errors, we can estimate the value of our expected value, $\hat{\theta}$. Hence, our objective is transferred to finding two more additional equations according to the fitting line to solve the non-homogeneous equation in Eq. 12.

[4]The experiments and explanations can be found in [2].

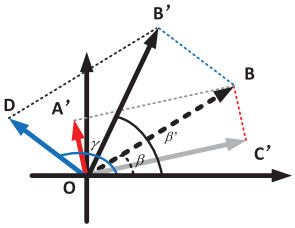

Fig. 6. Model of the signals.

Equation I: Intuitively, the first equation we built is one of the equations in Eq. 19:

$$\kappa = \Delta\hat{\theta} + e_1 \tag{20}$$

Note that another equation in Eq. 19 has the same effect as Eq. 20. We can utilize either of them.

Equation II: As shown in Fig. 4(b), the points y_n on the fitting line have a gap with the reported phase β_n. We define the difference between each pair of y_n and β_n as *residual error* S_n, *i.e.* :

$$S_n = y_n - \beta_n, \quad n = 1, 2, 3 \ldots N \tag{21}$$

According to the Eq. 19, the residual error S_n can be transformed into another expression, *i.e.*, the second desired equation:

$$S_n = n \cdot e_1 + e_2 - \hat{\alpha}_n, \quad n = 1, 2, 3 \ldots N \tag{22}$$

With Equ. 20 and 22, we can solve all the unknown variables in matrix x, including the mirror image phase $\hat{\theta}$ and the multipath variable $\hat{\alpha}$. Since $\hat{\theta} = (\theta + \hat{k} \cdot \pi) \ mod \ 2\pi$ (Eq. 9), the clean phase θ has two feasible solutions. However, the value of clean phase θ is limited by the received phase β: $\angle BOC' = (\theta - \beta) \ mod \ 2\pi < \frac{\pi}{2}$. Hence we can determine the solution of θ that meets such a requirement.

C. RSS Calculation

Besides phases, the measured RSS profile is not reliable as well. We conduct an experiment to explain it. We ask a volunteer to push her right hand in a crowded lab, and use a Kinect to capture the movement trajectory (as shown in Fig. 5). According to the movement trajectory obtained by the Kinect, we further calculate the phase profile of this activity (as shown in the top figure in Fig. 5(c)). Obviously, the received RSS cannot accurately reflect the tendency of the movement (as shown in the bottom figure in Fig. 5(c)).

Our basic idea towards this problem is utilizing the geometrical relationship of the measured RSS and the clean one, to infer the LOS RSS $\overrightarrow{OC'}$ and the human interference signal strength $\overrightarrow{OD}$. The LOS RSS (clean RSS) is an important parameter in many applications, such as tag localization, object state sensing, etc. And the human interference signal strength is introduced by the human movement, which is very useful for human activity detection and movement tracking. In many applications, a behaviour/movement detection algorithm uses the RSS changes to infer certain types of behaviours [18], [21]. With the two important values, CPIX can extend its applicability and practicability effectively.

Recall the example in Fig. 6 and Fig, 3, $\overrightarrow{OC'}$ is the LOS signal, $\overrightarrow{OA'}$ is the combined multipath signal, and $\overrightarrow{OD}$ is a dynamic multipath signal introduced by movements. Observing the rectangle $OA'BC'$, we can obtain the value of β by measuring the received phase at the reader, and calculate θ with the method proposed in the last section. And α' has a $(\frac{\pi}{2} + k_0 \cdot \pi)\ mod\ 2\pi$ difference with θ (Eq. 4). If we can determine the odevity of k_0, we can get access to the exact value of α'. To achieve this goal, we tell the odevity of k_0 by analysing the value of $\hat{\alpha}$, which is one of the unknown variables in matrix x. According to Eq. 9, k_0 has a following relationship with $\hat{\alpha}$, *i.e.* :

$$\tan\hat{\alpha} = (-1)^{k_0} \cdot (|\overrightarrow{OA'}|/|\overrightarrow{OC'}|), \tag{23}$$

since $|\overrightarrow{OA'}|/|\overrightarrow{OC'}| \leq 0$, we can further draw a conclusion that:

$$\begin{cases} \alpha' = \theta + \frac{\pi}{2},\ and\ k_0 = 2 \cdot m & \tan\hat{\alpha} < 0 \\ \alpha' = \theta + \frac{3\pi}{2},\ and\ k_0 = 2 \cdot m + 1 & \tan\hat{\alpha} \geq 0, \end{cases} \tag{24}$$

where m is a non-negative integer. We have known the value of $\hat{\alpha}$ when solving the equation set $A \cdot x = b$. Put it in the aforementioned equation, we will get the value of angle α'.

Now all the required parameters are ready for calculating the LOS RSS $\overrightarrow{OC'}$. We have obtained the values of θ, β and α'. The amplitude of $\overrightarrow{OB}$ can be easily calculated by the measured RSS. In the rectangle $OA'BC'$, the above information are enough to calculate the amplitude of LOS RSS $\overrightarrow{OC'}$ according to Edge and Side axioms (ASA) [48].

Except for the LOS RSS, we can also calculate the dynamic phase changes due to human interferences, namely the dynamic multipath signal $\overrightarrow{OD}$. As shown in Fig. 6, the phase of the new multipath signal is γ, and its amplitude is $|\overrightarrow{OD}|$. With the new reflector, the received signal $\overrightarrow{OB}$ will change to a re-construct one, denoted as $\overrightarrow{OB'}$ and shown in Fig. 6. By simply observing the change of the measured RSS ($\overrightarrow{OB}$ to $\overrightarrow{OB'}$), one may find that there is little difference. However the actual RSS introduced by the behaviour could be large ($|\overrightarrow{OD}|$). That maybe the reason that the measured RSS at the reader is not quite accurate to reflect the human movement. To obtain the pure influence of the moving object, we should estimate the related information, including the RSS and phase, of the new signal $\overrightarrow{OB'}$. Observing the example in Fig. 6, we have known the amplitude of two edges of triangle $\Delta OBB'$, namely $|OB|$ and $|OB'|$ by collecting the RSS before and after a moving object appears. In addition, we also know the received phase β and β'. According to Edge and Side axioms (SAS) [48], we can make sure the remaining edge, $\overrightarrow{BB'}$, which is a translational vector of $\overrightarrow{OD}$. $\overrightarrow{BB'}$ has the same length and orientation. As a result, we can calculate the phase λ and the amplitude of $\overrightarrow{OD}$ by solving the aforementioned triangle problem. Therefore the behaviour RSS can also be calculated.

V. Evaluation and Case Study

To thoroughly evaluate CPIX, we implement CPIX on COTS RFID devices and apply it to three mainstream RFID sensing applications, including tag localization, device calibration and human behavior sensing. We evaluate the performance of the three applications and compare them to the methods without CPIX.

A. Prototype Implementation

Hardware: the CPIX prototype includes **nothing more than the basic components** of a typical passive RFID system: an RFID reader, several directional antennas, a set of tags, and a backend server, which are all commodity devices. In specific, we use an ImpinJ Speedway R420 RFID reader, four Laird S9028PCL directional antennas, and four types of mainstream UHF passive RFID tags: ImpinJ E41C, E41B and Alien 9710, Alien 9640. Note it is usual for a reader to carry multiple antennas to improve the coverage, and the price of an antenna is much cheaper than the reader. The R420 reader operates at the UHF frequency band ($920.625 \sim 924.375$ MHz) and is able to hop over 16 channels. The gaps between two adjacent channels are the same, *i.e.*, 0.25 MHZ. The inventory mode is FM0, which can support about 380 successful queries per second. Each directional antenna has a gain of 8dBi and a size of $25\text{cm}\times25\text{cm}$. We run the software components of CPIX at a Dell desktop, which equips Intel Core i7-7700 CPU at 3.6 GHz and 16G memory. The ground truth data are obtained by laser range finder and Kinect, which are not required by CPIX.

Software: The backscatter communication of RFID uses two mainstream protocols, namely LLRP [49] and EPC Class 1 Generation 2 (C1G2) [50]. The reader communicates with passive tags according to EPC C1G2, and the reader reports the information back to the server based on LLRP. The CPIX software on the PC is implemented using $C^{\#}$.

B. Use Case 1: Tag Localization

Localization is the most commonly proposed RFID sensing application. It is also the basis of another important application, trajectory tracking. To emulate the practical environments, we conduct experiments in three different environments, *i.e.*, the "*hallway*" (HW), "*laboratory*" (Lab), and "*Office*" (OF), as shown in Fig. 7. In the three environments, multipath reflections exist and could be a critical factor that impacts the localization accuracy. Intuitively, the laboratory environment is considered to include more multipath reflectors than the hallway. Besides walls and grounds, many furniture like cabinet may be a strong reflector. While the office may contain even more multipath sources than the laboratory. The tagged items are placed among a mess of metal products like computer and screen, plastics, glasses and textile fabrics. **The Office environment is more complex than most environments used in existing work listed in Tables I.**

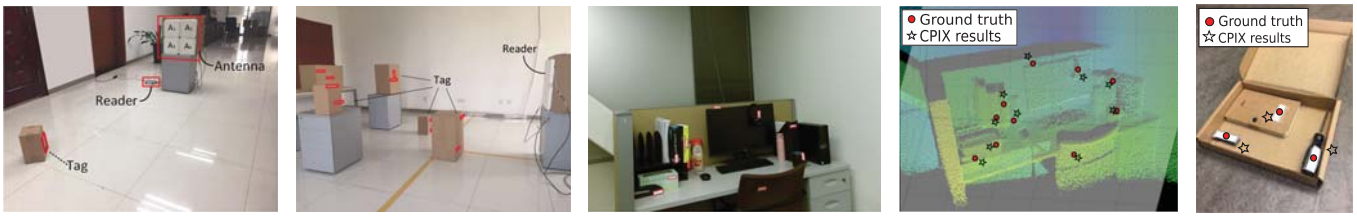

(a) Hallway (HW) (b) Laboratory (Lab) (c) Office (OF) (d) Results in Office (e) In a box

Fig. 7. Experiment environments and localization results of CPIX.

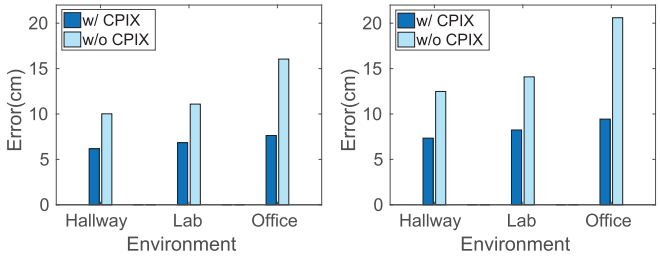

(a) No mobility (b) With mobility

Fig. 8. Mean localization errors.

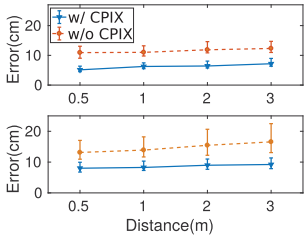

Fig. 9. Distance vs. Error.

We deploy 80 passive RFID tags in all. Among them, 12 are ImpinJ E41C tags, 40 are ImpinJ E41B tags, 20 are ALN-9710 and the other 8 are ALN-9640 tags, for the reader to localize. We utilize four antennas and form them as a square (as shown in Fig. 7). The coordinate origin of the deployment space is set as the center of this square. The tags we try to localize are at different positions. Their location varies among -82cm$\sim$16cm in height (z-axis), -89cm$\sim$104cm in width (y-axis), and 92cm$\sim$300cm in depth (x-axis). For the hallway experiments, in each round, only one tag is interrogated and the multipath effect is much weaker than that of the laboratory and office environment. While for laboratory/office environments, we place 20/10 tags in the area and localize all of them at the same time. For each environment, we conduct two sets of experiments. One is without moving objects and another has one volunteer keep walking arbitrarily in the area. The walking speed is 1$\sim$2m/s. We call these two setups as "*no mobility*" and "*with mobility*".

The localization algorithm is a recently developed Hyperbola-based Localization (HL) method introduced in [9], [11]. We do not change the existing localization algorithm and just feed the algorithm with two sets of phase data, because our objective is to evaluate the quality of the phase data reported by CPIX rather than a new localization method.

Localization errors. In Fig. 8, we show the mean localization errors of the HL algorithm when using the CPIX phase (w/ CPIX) and the phase data from the reader API (w/o CPIX) respectively. We find that CPIX evidently reduces the HL errors in all environments, with and without mobility. The error reduction rate in Hallway is 38.4% (10.02cm to 6.17cm) without mobility and 41.2% (12.48cm to 7.34cm) with mobility. The error reduction rate in Lab is 32.7% (11.09cm to 7.58cm) without mobility and 41.5% (14.09cm to 8.24cm) with mobility. The error reduction rate in Office is 52.5% (16.05cm to 7.63cm) without mobility and 54.2% (20.6cm to 9.43cm) with mobility. We find when the environment is more complex and includes mobility, the multipath are more significant and the error reduction using CPIX is more obvious.

We also test the ability of CPIX on penetrating obstacles. We put the tagged things in a paper box, and then close the box and try to localize the tags inside the box. The estimation results of CPIX are shown in Fig. 7(e). We find that though the box blocks the LOS signals and introduce more reflections, the localization errors are still acceptable in this case. In this case, CPIX shows **possibilities of localizing none-line-of-sight objects** with a COTS reader.

We compare the CPIX-enabled HL with some state-of-art localization schemes, including PinIt [17], RF-IDraw [11], Tagoram [12], BackPos [9], and RFly [27]. Note for all results in the table, the distance to the reader used in our experiments is no less than the corresponding distance of the results from these existing methods. The localization environments in our experiments are **no better** than other work. CPIX based localization provides the lowest errors in both the median and worst cases. As shown in Tab. III, most of those methods operate in low multipath environments or require extra hardware. Note that we do not include recent work such as Broadband Nonlinear Backscatter [26] and RFind [28] that use self-built devices. The former needs extra hardware like flying drones, and the later requires multiple USRP SNRs to build the SDR reader. We compare these SDR-supported methods, including the ultra-wide-band-based (UWB) method and beamforming-based method at the end of this part.

Distance versus error: We also investigate the relationship between localization error and tag distance to the antennas in the lab environment. We place 40 tags in 4 different distances: 0.5m, 1m, 2m, and 3m, each with 10 tags. The distance from the tag to the reader varies evenly in 0.5m to 3m. According to Fig. 9, the mean error by utilizing CPIX for 0.5m, 1m, 2m and 3m are 5.13cm, 6.26cm, 6.42cm and 7.18cm, respectively, which is much better than the original HL method (10.95cm, 11.01cm, 11.87cm, 12.32cm). In addition, CPIX works well even with one person moving around

TABLE III
COMPARISON OF STATE-OF-THE-ART RFID LOCALIZATION SCHEMES

Localization work	Extra hardware	Multipath-prevalent?	Dimension	Median error	Worst error
RF-IDraw [11]	Two readers	not allow	Three	19cm	60cm
Tagoram [12]	none	not allow	Two	12.3cm	$>$ 20cm
BackPos [9]	none	not allow	Two	12.8cm	$>$ 21cm
RFly [27]	Relay drones	allow	Three	19cm	$>$ 90cm
PinIt [17]	SDR, mobile ant., anchor tags	allow	Three	11.2cm	25cm
CPIX (HW/OF)	none	allow	Three	6.17cm/7.63cm	9.86cm/11.39cm

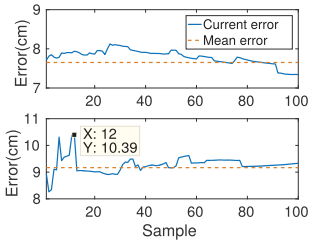

Fig. 10. Sample number vs. Error.

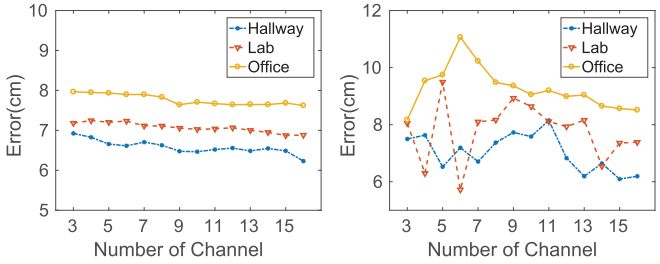

(a) No mobility (b) With mobility

Fig. 11. Channel number vs. Error.

(8.01cm, 8.27cm, 8.98cm, 9.22cm). CPIX can achieve a good localization accuracy even when the distance is 3m, which is considered to be far in most existing work.

Number of samples versus error: In our experiments, an RFID reader stays at each channel for a short time period. During this period, the reader is able to collect a number of samples of tag replies. We expect to use fewer samples yet achieve higher localization accuracy. We then observe the relationship between the number of samples and the localization error. In Fig. 10, we show the error in the office environment when utilizing the first M samples ($M = 1, 2, \ldots 100$). The top figure shows the errors in 'no mobility' case, while the bottom one shows the results with mobility. We find that the errors are stable without mobility, and vary from 7.34cm to 8.13cm. While for dynamic case, the errors fluctuate sharply before the first 12 samples, and quickly converge to the mean error. Note that in UHF passive RFID systems, the throughput of inventorying tags is very high. Normally a tag can report up to 380 samples to the reader per second. Hence CPIX only requires a trivial time for collecting phase data while providing a high localization accuracy.

Number of channels versus error. In CPIX, we may use up to all 16 channels. It is worth to investigate the minimum number of channels required for this method, considering that in some extreme applications the time duration for localizing a tag may be limited to allow a reader to traverse only a small number of channels. We then alter the number of channels from 3 to 16 involved in each experiment and show the results in Fig. 11. The left figure shows the results without moving person. We find that the mean error reduces slowly when the number of channels increases. Using only three channels could achieve a mean localization error $<$7cm. While the right one shows error variations with a person moving around. The errors fluctuate among channels. However, the error in the worst case is no larger than 8.15cm/9.49cm/11.06cm in HW/Lab/OF environments.

Number of antenna versus error: In fact, CPIX has the opportunity to use less equipment. We conduct an experiment to demonstrate the performance of CPIX when we just use one antenna. Note that the hyperbola-based localization method (HL) needs four antennas. In this experiment, we purely show the phase errors. In our experiments, we utilize an RFID reader and one antenna. Three ImpinJ H47 tags are placed in front of the antenna. We change the separation distances between the antenna and the tags from 0.2m to 1.8m. To remove unknown factors like the initial phases of the antenna and tags, we treat the phase value of 0.2m as a baseline.

Two experiments are conducted to evaluate the performance of CPIX. The first one is to exhibit the performance of CPIX in different static environments. We place the tag-antenna system in three positions. The surrounding environments of these positions are totally different. We exhibit the phase errors of the raw data (w/o CPIX) and the ones measured with CPIX in Table. IV. According to Table. IV, CPIX can reduce the phase error by 0.14% to 12.61%. The second experiment is to evaluate the performance of CPIX in coping with dynamic multipath effects. We ask a volunteer to walk around (scenario a) or walk through (scenario b) the tag-antenna system. In the former one, the moving volunteer will provide unpredictable dynamic multipath effects, while in the latter one, the LOS (Line-of-Sight) path will be intermittently blocked by the human body. The phase errors of the second experiment are shown in Table. V. We find that CPIX can significantly improve the accuracy by 18.12% (scenario a) and 25.28% (scenario b). Hence CPIX is effective even with only one antenna.

Compared with UWB-based methods. We also compare CPIX with some ultra-wide-band-based (UWB) localization methods, *e.g.*, RFind [28]. RFind can emulate over 220 MHz of bandwidth on tags designed with a communication bandwidth of only tens to hundreds of kHz. Combined with some super-resolution algorithm over this bandwidth, RFind achieves a median accuracy of 0.91 cm in 2D localization.

TABLE IV
MEAN ERRORS OF PURE PHASES ($0\sim 2\pi$) VS. POSITIONS

Position	Distance (m)	0.4	0.6	0.8	1	1.2	1.4	1.6	1.8
1	w/o CPIX	0.1274	0.3770	0.7374	1.0053	0.4843	0.8469	1.0998	1.1522
	w/ CPIX	0.1208	0.3634	0.7103	0.9826	0.4511	0.8563	1.0964	1.1480
2	w/o CPIX	0.5326	1.3992	1.0486	1.1688	0.7961	1 0857	1.9326	2.1094
	w/ CPIX	0.5216	1.3973	1.0281	1.1643	0.7797	1.0861	1.9835	2.1006
3	w/o CPIX	0.4924	0.4395	0.2530	0.8143	0.8281	0.4599	0.8676	0.4413
	w/ CPIX	0.4979	0.4313	0.2211	0.8066	0.8111	0.4659	0.8252	0.5016

TABLE V
MEAN ERRORS OF PURE PHASES ($0\sim 2\pi$) VS. SCENARIOS

Scenarios	Distance (m)	0.4	0.6	0.8	1	1.2	1.4	1.6	1.8
a)	w/o CPIX	0.6758	0.4819	0.2259	0.7824	0.9876	0.3109	0.5101	0.7682
	w/ CPIX	0.6684	0.3747	0.1382	0.7088	0.8436	0.2302	0.4353	0.7731
b)	w/o CPIX	0.4262	0.4772	0.4490	0.8050	1.0558	0.6885	0.4085	1.3565
	w/ CPIX	0.1707	0.4452	0.4814	0.7079	1.1245	0.4675	0.2588	1.2992

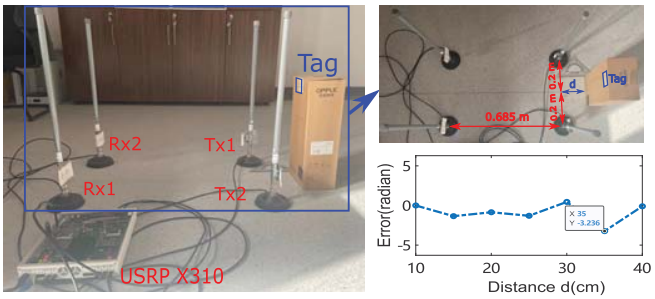

Fig. 12. The deployment and experiment results of beamforming-based localization.

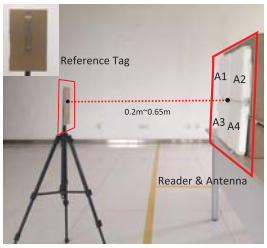

Fig. 13. Experiment setup.

However, the commercial RFID reader has no ability to implement ultra-band localization or transmit with a larger bandwidth. Hence, RFind employs two Software-Defined-Radio-based (SDR) RFID readers and an external clock (about $8000 in total). On the contrary, CPIX based localization does not need any extra hardware or training procedure and works well in multipath-prevalent environments. According to the experiment results in Table. V-B, the median accuracy of CPIX is 2.95 cm even with a person walking around. Hence, CPIX can provide not-bad localization accuracy with only one COTS RFID reader and a single antenna (about $1700 in total), which is very cost-efficient.

Compared with Beamforming-based methods. We also conduct experiments to compare the localization performance of beamforming-based methods and CPIX. As shown in Fig. 12, we implement a 2×2 MIMO SDR-based RFID system, which employs a USRP X310 and four omnildirectional antennas. An ImpinJ H47 tag is placed along the center line of the antennas and is moved from 0.1 m to 0.4 m, with a step of 0.05 m. Under this circumstance, the phase over distance, *i.e.*, θ_D, are the same. To calibrate the two receiver antennas, we use the $\Delta\theta$ at 0.1 m as the baseline. As shown in Fig. 12, the maximum phase error reaches -3.24, and the mean phase error is about -0.913, which will lead to a localization error of 4.72 cm. However, with CPIX, the mean phase error is 0.38 (according to the results in Table. IV), which outperforms the beamforming-based phase measurement.

C. Use Case 2: Device Calibration

RFID devices are diverse in their hardware characteristics, leading to inconsistency in their physical features, such as phase, amplitude, and frequency. For example, we have to know the initial phase offset of an RFID reader antenna and then remove it to accurately calculate the phase of a target tag. We call this process as *device calibration*.

Device calibration aims to eliminate the initial phase differences between different antennas, which can be achieved during the execution of CPIX algorithm. The traditional antenna calibration method is to collect the phases of a reference tag, which is deployed on the perpendicular bisector of two antennas. According to Eq. 25, for antenna i and j their received phases of the given reference tag can be expressed as a sum of three parts, *i.e.* :

$$\theta_i = \theta_D^i + \theta_{A_i} + \theta_T, \theta_j = \theta_D^j + \theta_{A_j} + \theta_T \tag{25}$$

where θ_i and θ_j represent the received phases of the reference tag with antenna i and j respectively and θ_{A_i} and θ_{A_j} are the antenna phase offsets. Since the reference tag is on the bisector of two antennas, the phases of distance θ_D^i and θ_D^j are the same for different antennas. The initial phase θ_T keeps identical for a same tag. Hence

$$\Delta\theta_{ij} = \theta_{A_i} - \theta_{A_j} = \theta_i - \theta_j \tag{26}$$

Note that it is extremely hard to retrieve the true value of an antenna's initial phase. Instead, we can calculate such a phase difference $\Delta\theta_{ij}$ between two antennas. That is why many prior phase based applications [9], [12], including the

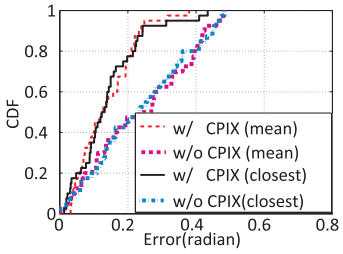

Fig. 14. The calibration error.

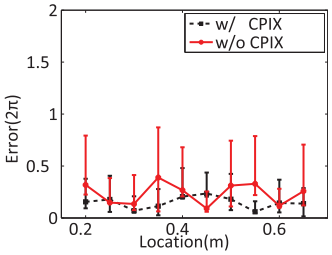

Fig. 15. Distance vs. Error.

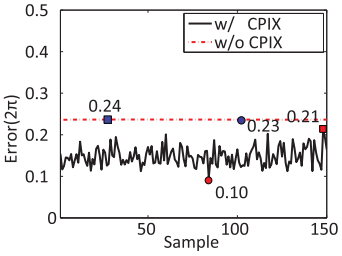

Fig. 16. Number of samples vs. Error.

TABLE VI
THE SIMILARITY OF GROUND TRUTH SIGNAL AND THE SIGNALS WITH/WITHOUT CPIX

Method	RSS	Phase
Raw data	30.18%	72.66%
with CPIX	89.26%	82.17%

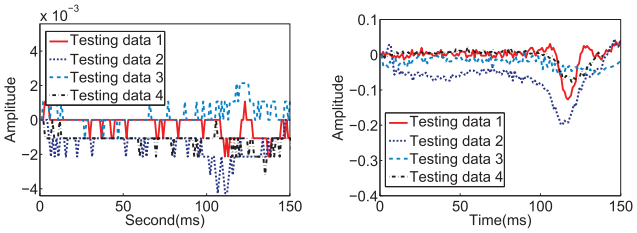

(a) Raw RSS (b) RSS estimated by CPIX

Fig. 17. RSS profiles of human movements.

tag localization and human behaviour sensing, utilize $\Delta\theta_{ij}$ as the essential objective for device calibration.

We use CPIX to estimate the accurate value of $\Delta\theta_{ij}$. As shown in Fig. 13, we place a reference tag the axis orthogonal to the center of the square formed by four reader's antennas, and vary the distance using 10 different positions. The distance of the reference tag from the center of the antennas ranges from 0.2m to 0.65m. We conduct our experiments in the laboratory environment, and let the reader go through all the channels. In each channel, we collect the phase of the reference tag without CPIX for 5 seconds. We examine the performance of CPIX from two aspects: the calibration error for tags with fixed positions, and calibration error when we change the distance between the tag and antennas.

The calibration error: We define the calibration error e as follows:

$$e = \Delta\hat{\theta}_{ij}^{p} - \Delta\theta_{ij}^{base} \tag{27}$$

where $\Delta\hat{\theta}_{ij}^{p}$ represents the calculated value of $\Delta\theta_{ij}$ for each position p. Due to the influence of surrounding environment, $\Delta\hat{\theta}_{ij}^{p}$ are different at different positions. $\Delta\theta_{ij}^{base}$ is the value that we used as the final report of $\Delta\theta_{ij}$. In our experiments, we use two candidates of $\Delta\theta_{ij}^{base}$, respectively. One is the phase of the closest position (0.2m), *i.e.*, $\Delta\theta_{ij}^{1}$. The other is the mean value of all the phases calculated at 10 positions. Obviously, if the calibration is accurate, e should be very small. Fig. 14 shows the cumulative distribution of the calibration errors with/without CPIX. The median errors with CPIX are $0.12 \cdot 2\pi$ (closest) and $0.13 \cdot 2\pi$ (mean), respectively. While the median errors without CPIX are $0.25 \cdot 2\pi$ (closest) and $0.23 \cdot 2\pi$ (mean). The results indicate that CPIX enable nearly 50% error reduction for device calibration.

Distance versus Error. We observe the change of e when varying the distance between the reader and the reference tag. Fig. 15 shows the error range and the mean error with/without CPIX for all 10 positions. The mean errors with CPIX are from $0.06 \cdot 2\pi$ to $0.24 \cdot 2\pi$. While the mean errors without CPIX are from $0.09 \cdot 2\pi$ to $0.39 \cdot 2\pi$. Obviously, CPIX shows significant advantage even if we enlarge the distance between the reader and tags. CPIX extends the effective operating range of device calibration.

Number of Samples versus Error. We also evaluate the error with increased number of samples in device calibration. We show that the errors of using the first M (M=1,2,3,…150) samples in our algorithm in Fig. 16. According to Fig. 16, we find that the number of samples do not affect the final error, similar to the situation in the localization. Therefore, CPIX can improve device calibration very efficiently and effectively.

D. Use Case 3: Human Activity Sensing

To evaluate the performance of CPIX on combating multipath effects in human activity sensing, we conduct two sets of experiments. The first is validating CPIX on accurately retrieving human activities. The second one is applying CPIX to an existing activity sensing system, RFIPad [21].

Accurately retrieving the human activity. We also conduct experiments to exhibit the performance of CPIX on RSS estimation. We ask a volunteer to sit in front of an RFID antenna. An RFID tag is placed between the volunteer and the antenna. The volunteer pushes and pulls her hand four times. We exhibit the raw RSS and the one extracted by CPIX in Fig. 17(a) and 17(b), respectively. We find that the raw RSS has a low resolution, which is insufficient for human movement monitoring. While with CPIX, we can observe clear signal profiles.

Fig. 18. Experiment deployment.

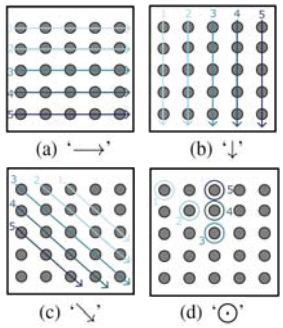

Fig. 19. Five hand trajectories of four strokes. (a) Move from left to right. (b) Move from top to bottom. (c) Move from top left corner to bottom right corner. (d) Push the hand.

To further evaluate CPIX in a mathematical way, we ask two volunteers to perform three activities, namely pushing hands, pulling hands and raising legs. To evaluate the performance of CPIX on coping with multipath effects, we conduct the experiments in three different places. At all these places, the volunteer is surrounded by many strong reflectors, including several metal cabinets, tables, and other furniture. We use a Kinect to capture the ground truth of the movement paths of the activity. In tab. VI, we exhibit the similarity among the ground truth and the RSS and phase signals with or without CPIX. We find that the raw data can hardly reflect human activity, especially the RSS profile. While CPIX can significantly improve the similarity even in multipath-prevalent environments. So CPIX can accurately retrieve the human movement trajectory in different environments, which may improve the accuracy and practicability of the human activity sensing system.

Apply CPIX in state-of-the-art sensing system. We also apply CPIX to a state-of-the-art human behavior sensing work, RFIPad [21], and evaluate its performance. RFIPad is a human hand gesture detection system, which can recognize touch-pad actions and 26 English letters by detecting every stroke people "write" in the air. As shown in Fig. 12, we form 25 tags in a 5×5 array, with an equal interval of 6cm. People can perform in-air handwriting on the virtual screen. We employ the same experiment deployment in the RFIPad work: a directional antenna placing face the tag array with a people in-between. In fact, some of the English letters are similar to each other, *e.g.*, 'H' and 'A', 'X' and 'V', 'P' and 'D', *etc.*. As a result, detecting every stroke accurately is necessary for letter recognition. We choose four kinds of typical strokes, namely '⟶', '↓', '↘', '⊙ (click)'. As shown in Fig. 19, for every stroke, we choose five possible hand trajectories (or positions). We repeat each hand trajectory for 10 times and determine which gesture the person performs. To observe the influences of multipath effects on system performance, we place the system in a crowded office room. We employ the same recognition algorithm proposed in RFIPad and feed it with the data with or without CPIX. Note that RFIPad may use either the phase or RSS data. Hence we compare the recognition accuracy of both directly measured data (w/o CPIX) and CPIX data (with CPIX) when utilizing phase or RSS. The recognition accuracy of RFIPad with/ without CPIX is exhibited in Table VII, which shows that employing CPIX can improve the recognition accuracy significantly. In most situations, CPIX can improve the accuracy to around 90% compared to the original accuracy (70%-80%).

TABLE VII
ACCURACY OF RFIPAD WITH/WITHOUT CPIX

Data	CPIX	⟶	↓	↘	⊙
RSS	w/o	60%	73.33%	80%	73.33 %
	w/	80%	86.67%	86.67%	93.33%
Phase	w/o	73.33%	86.67%	80 %	86.67%
	w/	80%	93.33%	86.67%	93.33%

E. Benchmarks About the Tag Reading Rates

Efficient tag reading is very important in our experiments. Hence we elaborate some benchmarks of the tag reading rates when we use different system settings. According to the results, we can draw a sketch about the system settings that may improve the tag reading rate. In the following part, we will exhibit the benchmarks by trying different parameters, including the modulation scheme, the transmission power, the tag number, *etc.*. In these experiments, we deploy multiple tags with a distance of 10 cm to the RFID antenna. The transmission power is 32 dB and the session number is 2. We run the reader for 10 seconds and calculate the average reading rate, which is defined as the reads (♯) per second.

Modulation schemes. RFID tag encodes its backscattered data with either FM0 baseband or Miller modulation. The modulation scheme determines how many symbols are needed to represent one data bit. Among these modulation schemes, 1 symbol is needed for FM0, while 4 and 8 symbols are needed for Miller 4 (M4) and Miller 8 (M8). Intuitively, the fewer symbols that are needed for representing one bit, the more efficient the communication will be. Our experiment results confirm our conclusion. With FM0, the reader can obtain 369 success responses per second from 10 tags. While for M4 and M8, the reading rates decrease to 192 and 127, respectively. Hence, choosing an appropriate modulation scheme is an effective way to improve the reading rates.

The transmission distance. The transmission distance between the reader antenna and the tags may also impact the reading rate. In our experiment, we utilize two tags and put them in front of an antenna with a distance from 5 cm to 3 m. As shown in Fig. 20(b), when the separation distance is from 5 cm to 1 m, the reading rates keep stable. While when the distance increases to 2 m or further, the reading rate decreases sharply.

The population estimation. The ImpinJ reader allows users to set a parameter called the tag population. Correct estimation

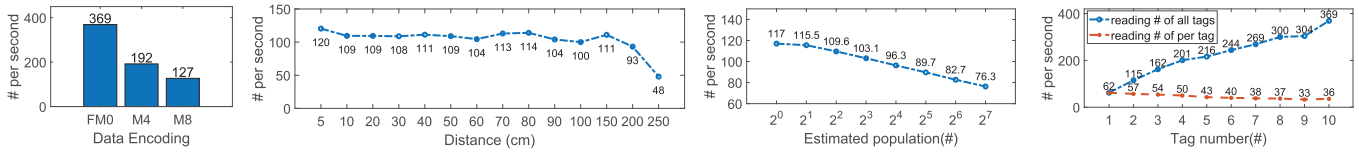

(a) Modulation scheme (b) Distance (c) Estimation of tag's number (d) Tag number

Fig. 20. Some factors that may impact the reading rate.

of the tag population can help the reader to set an appropriate slot number. Prior researchers have proved that when the slot number equals the number of tags, the throughput will reach the peak. In our experiment, we use two tags and set the population number from 2^0 to 2^7. Absolutely, when the slot number equals 2^1, the communication is the most efficient. As shown in Fig. 20(c), the reading rates decrease by about 6.5/s when the estimated population increases by two times. The reasons may be two folds: 1) the time duration of an entire slot (with one tag's response) is much longer than that of an empty one. 2) once the reader realizes that the population estimation is not reliable, it will send the 'QuaryAdjust' command, which can stop the current inventory and inform the tags with an appropriate slot number. Hence the knowledge about the tag number is also important in improving the reading rate.

Tag number. The number of tags also introduce non-negligible influences in the reading. Intuitively, increasing the number of tags will lead to reading rate decreases of each tag, but increases of all tags. We utilize 1 to 10 tags in our experiments and observe their reading rates. As shown in Fig. 20(d), the reads per tag within one second will decrease from 62/s to 36/s. However, when we read 10 tags at the same time, the reader can obtain 369 success responses.

The transmission frequency. We also conduct some experiments and observe the reading rates when altering the reader's channel. We find that the reading rates in different channels are relatively stable. For two tags, the reader can obtain 114∼116 success responses for all channels. Hence we can safely infer that the transmission frequency may not affect the reading rate.

VI. Discussion

In our design and experiments, we employ a frequency-fixed reader, which can transmit a fixed frequency and hop to another one under control. However, in some regions over the world, the FCC mandates that the RFID readers should hop its frequency periodically and pseudo-randomly. As a result, the data at one frequency may be collected at the different time periods, and intuitively, have inconsistent outside environments. In fact, our design is compatible with frequency-hopping readers. That is because: 1) We do not have any assumptions on the frequency hopping mode. On the contrary, we also consider the differences introduced by the transmitting frequency. 2) The communication between the RFID reader and tags is much more frequent than the alteration of outside environments. An RFID reader can obtain up to 400 successfully responses in just one second. However, only several dozens of data is sufficient for our algorithm (as described in Sec. V-B). The changes of the environment during such a small time period can be ignored.

VII. Current Limitations

CPIX has its own limitations in clean information extraction. We discuss a few points here.

A. Solid Static Obstacles (None-Line-of-Sight Cases)

CPIX focus on extracting the line-of-sight signals from the raw signals. However, if a solid static obstacle blocks the LOS propagation path, the received signals are all composed by multipath parts. In this case, the received signals of the tag do not contain a LOS one, not to mention figure it out. However, if the obstacle is temporary, *i.e.*, a walking person block the LOS path for a moment, CPIX can also work well. That is because the received data that changes sharply due to the human movements will be considered as outliers in our algorithm.

B. Tag Mobility

Another limitation is that the target tag should not move during channel shifting. That is because the LOS signal will not keep identical if the target tag moves. In addition, with the tag movement, the multipath effects will also change timely. However, if we can obtain the movement trajectory of the target tag (in some cases, the tagged objects follow a determined trajectory, *e.g.*, items on conveyor belts in airports and factories), we can also estimate the LOS signals. In addition, according to the discovery in prior researches [51], the multipath-effects are similar within a small range ($\approx$ 11cm). As a result, CPIX may have possibility to cope with slight tag mobilities in some cases.

C. Data Quality

In our experiments, we find that if the outside environment is very stable, *i.e.*, the multiple effects are mainly arisen by the static reflectors, the performance of CPIX is highly related to the data quality. In other words, if the raw data is very accurate, CPIX will perform well. On the contrary, CPIX may not provide good estimation results

D. The Fidelity of Our Design

In our algorithm, the performance depends on the precise estimation of the fitting line. However, the estimation is mainly determined by currently collected data. If the dynamic multipath signals do not comply the only assumption in our algorithm, *i.e.*, $\sum_{n=1}^{N} \omega_n \cdot \hat{\alpha}_n^d \approx 0$, a bad performance will occur.

VIII. Conclusion

In this paper, we present CPIX, the first generalized and low-cost solution to calculate accurate clean physical information for RFID sensing in the practical multipath-prevent environment. We use a new signal analysis model to extract the clean physical information using multi-channel measurement. We study three use cases of CPIX: tag localization, device calibration and human behaviour sensing. The experiments indict that CPIX can achieve good accuracies even with moving objects. So CPIX has the potential to improve numerous RFID sensing applications that rely on phase or RSS measurement. Our future work will further explore more CPIX-aided sensing applications.

References

[1] X. Li, M. Wang, H. Wang, Y. Yu, and C. Qian, "Toward secure and efficient communication for the Internet of Things," *IEEE/ACM Trans. Netw.*, vol. 27, no. 2, pp. 621–634, Apr. 2019.

[2] Q. Lin, L. Yang, H. Jia, C. Duan, and Y. Liu, "Revisiting reading rate with mobility: Rate-adaptive reading in COTS RFID systems," in *Proc. ACM CoNEXT*, 2017, pp. 199–211.

[3] X. Li, M. Wang, S. Shi, and C. Qian, "VERID: Towards verifiable IoT data management," in *Proc. ACM/IEEE IoTDI*, Apr. 2019, pp. 118–129.

[4] H. Jin, J. Wang, Z. Yang, S. Kumar, and J. Hong, "WiSh: Towards a wireless shape-aware world using passive RFIDs," in *Proc. ACM MobiSys*, 2018, pp. 428–441.

[5] H. Li, P. Zhang, S. Al Moubayed, S. N. Patel, and A. P. Sample, "ID-match: A hybrid computer vision and rfid system for recognizing individuals in groups," in *Proc. ACM CHI*, 2016, pp. 4933–4944.

[6] G. Wang *et al.*, "A (Near) zero-cost and universal method to combat multipaths for RFID sensing," in *Proc. IEEE 27th Int. Conf. Netw. Protocols (ICNP)*, Oct. 2019, pp. 1–4.

[7] H. Cai, G. Wang, X. Shi, J. Xie, M. Wang, and C. Qian, "When tags 'read' each other: Enabling low-cost and convenient tag mutual identification," in *Proc. IEEE ICNP*, Oct. 2019, pp. 1–11.

[8] X. Shi *et al.*, "TagAttention: Mobile object tracing without object appearance information by vision-RFID fusion," in *Proc. IEEE 27th Int. Conf. Netw. Protocols (ICNP)*, Oct. 2019, pp. 1–11.

[9] T. Liu, L. Yang, Q. Lin, Y. Guo, and Y. Liu, "Anchor-free backscatter positioning for RFID tags with high accuracy," in *Proc. IEEE Conf. Comput. Commun. (INFOCOM)*, Apr. 2014, pp. 379–387.

[10] S. Azzouzi, M. Cremer, U. Dettmar, R. Kronberger, and T. Knie, "New measurement results for the localization of UHF RFID transponders using an angle of arrival (AoA) approach," in *Proc. IEEE Int. Conf. RFID*, Apr. 2011, pp. 91–97.

[11] J. Wang, D. Vasisht, and D. Katabi, "RF-IDraw: Virtual touch screen in the air using RF signals," in *Proc. ACM SIGCOMM*, 2014, pp. 235–246.

[12] L. Yang, Y. Chen, X. Li, C. Xiao, M. Li, and Y. Liu, "Tagoram: Real-time tracking of mobile RFID tags to high precision using COTS devices," in *Proc. ACM MOBICOM*, 2014, pp. 237–248.

[13] L. Shangguan, Z. Li, Z. Yang, M. Li, and Y. Liu, "OTrack: Order tracking for luggage in mobile RFID systems," in *Proc. IEEE INFOCOM*, Apr. 2013, pp. 3066–3074.

[14] L. Shangguan, Z. Yang, A. X. Liu, Z. Zhou, and Y. Liu, "Relative localization of RFID tags using spatial-temporal phase profiling," in *Proc. USENIX NSDI*, 2015, pp. 251–263.

[15] L. Yang, Q. Lin, X. Li, T. Liu, and Y. Liu, "See through walls with COTS RFID system!" in *Proc. 21st Annu. Int. Conf. Mobile Comput. Netw.*, Sep. 2015, pp. 487–499.

[16] L. Shangguan, Z. Zhou, X. Zheng, L. Yang, Y. Liu, and J. Han, "ShopMiner: Mining customer shopping behavior in physical clothing stores with COTS RFID devices," in *Proc. ACM SenSys*, 2015, pp. 113–125.

[17] J. Wang and D. Katabi, "Dude, where's my card?: RFID positioning that works with multipath and non-line of sight," in *Proc. ACM SIGCOMM*, 2013, pp. 51–62.

[18] H. Ding *et al.*, "Device-free detection of approach and departure behaviors using backscatter communication," in *Proc. ACM Int. Joint Conf. Pervasive Ubiquitous Comput.*, Sep. 2016, pp. 167–177.

[19] H. Ding *et al.*, "FEMO: A platform for free-weight exercise monitoring with RFIDs," in *Proc. ACM SenSys*, 2015, pp. 141–154.

[20] T. Wei and X. Zhang, "Gyro in the air: Tracking 3D orientation of batteryless Internet-of-Things," in *Proc. ACM Mobicom*, 2016, pp. 55–68.

[21] H. Ding *et al.*, "RFIPad: Enabling cost-efficient and device-free in-air handwriting using passive tags," in *Proc. IEEE 37th Int. Conf. Distrib. Comput. Syst. (ICDCS)*, Jun. 2017, pp. 447–457.

[22] J. Liu, M. Chen, S. Chen, Q. Pan, and L. Chen, "Tag-compass: Determining the spatial direction of an object with small dimensions," in *Proc. IEEE Conf. Comput. Commun. (INFOCOM)*, May 2017, pp. 1–9.

[23] S. Pradhan, E. Chai, K. Sundaresan, L. Qiu, M. A. Khojastepour, and S. Rangarajan, "RIO: A pervasive RFID-based touch gesture interface," in *Proc. ACM Mobicom*, 2017, pp. 261–274.

[24] D. Vasisht, G. Zhang, O. Abari, H.-M. Lu, J. Flanz, and D. Katabi, "In-body backscatter communication and localization," in *Proc. Conf. ACM Special Interest Group Data Commun.*, Aug. 2018, pp. 132–146.

[25] L. Shangguan and K. Jamieson, "The design and implementation of a mobile RFID tag sorting robot," in *Proc. 14th Annu. Int. Conf. Mobile Syst., Appl., Services*, Jun. 2016, pp. 31–42.

[26] Y. Ma, X. Hui, and E. C. Kan, "3D real-time indoor localization via broadband nonlinear backscatter in passive devices with centimeter precision," in *Proc. 22nd Annu. Int. Conf. Mobile Comput. Netw.*, Oct. 2016, pp. 216–229.

[27] Y. Ma, N. Selby, and F. Adib, "Drone relays for battery-free networks," in *Proc. Conf. ACM Special Interest Group Data Commun.*, Aug. 2017, pp. 335–347.

[28] Y. Ma, N. Selby, and F. Adib, "Minding the billions: Ultra-wideband localization for deployed RFID tags," in *Proc. ACM MobiCom*, 2017, pp. 248–260.

[29] L.-X. Chuo, Z. Luo, D. Sylvester, D. Blaauw, and H.-S. Kim, "RF-echo: A non-line-of-sight indoor localization system using a low-power active RF reflector ASIC tag," in *Proc. ACM MobiCom*, 2017, pp. 222–234.

[30] Z. Luo, Q. Zhang, Y. Ma, M. Singh, and F. Adib, "3D backscatter localization for fine-grained robotics," in *Proc. USENIX NS*, 2019, pp. 765–782.

[31] R. O. Schmidt, "Multiple emitter location and signal parameter estimation," *IEEE Trans. Antennas Propag.*, vol. 34, no. 3, pp. 276–280, Mar. 1986.

[32] J. Wang, F. Adib, R. Knepper, D. Katabi, and D. Rus, "RF-compass: Robot object manipulation using RFIDs," in *Proc. ACM MobiCom*, 2013, pp. 3–14.

[33] Y. Zhao, Y. Liu, and L. M. Ni, "VIRE: Active RFID-based localization using virtual reference elimination," in *Proc. Int. Conf. Parallel Process. (ICPP)*, Sep. 2007, p. 56.

[34] A. Parr, R. Miesen, and M. Vossiek, "Inverse SAR approach for localization of moving RFID tags," in *Proc. IEEE Int. Conf. RFID (RFID)*, Apr. 2013, pp. 104–109.

[35] R. Miesen, F. Kirsch, and M. Vossiek, "Holographic localization of passive UHF RFID transponders," in *Proc. IEEE Int. Conf. RFID*, Apr. 2011, pp. 32–37.

[36] G. Wang *et al.*, "HMRL: Relative localization of RFID tags with static devices," in *Proc. 14th Annu. IEEE Int. Conf. Sens., Commun., Netw. (SECON)*, Jun. 2017, pp. 1–9.

[37] L. Shangguan, Z. Zhou, and K. Jamieson, "Enabling gesture-based interactions with objects," in *Proc. 15th Annu. Int. Conf. Mobile Syst., Appl., Services*, Jun. 2017, pp. 239–251.

[38] L. Yang, Y. Qi, J. Fang, X. Ding, T. Liu, and M. Li, "Frogeye: Perception of the slightest tag motion," in *Proc. IEEE Conf. Comput. Commun. (INFOCOM)*, Apr. 2014, pp. 2670–2678.

[39] F. Adib, Z. Kabelac, and D. Katabi, "Multi-person localization via RF body reflections," in *Proc. USENIX NSDI*, 2015, pp. 279–292.

[40] W. Jiang *et al.*, "Towards environment independent device free human activity recognition," in *Proc. 24th Annu. Int. Conf. Mobile Comput. Netw.*, Oct. 2018, pp. 289–304.

[41] M. Bouet and A. L. dos Santos, "RFID tags: Positioning principles and localization techniques," in *Proc. 1st IFIP Wireless Days*, Nov. 2008, pp. 1–5.

[42] H. Jin, Z. Yang, S. Kumar, and J. I. Hong, "Towards wearable everyday body-frame tracking using passive RFIDs," *Proc. ACM Interact., Mobile, Wearable Ubiquitous Technol.*, vol. 1, no. 4, pp. 1–23, 2018.

[43] W. Wang, A. X. Liu, and K. Sun, "Device-free gesture tracking using acoustic signals," in *Proc. 22nd Annu. Int. Conf. Mobile Comput. Netw.*, Oct. 2016, pp. 82–94.

[44] D. Vasisht, S. Kumar, and D. Katabi, "Decimeter-level localization with a single WiFi access point," in *Proc. USENIX NSDI*, 2016, pp. 165–178.

[45] S. K. Islam and M. R. Haider, *Sensors and Low Power Signal Processing*. Springer, 2009.

[46] L. Klozar and J. Prokopec, "Propagation path loss models for mobile communication," in *Proc. 21st Int. Conf. Radioelektronika*, Apr. 2011, pp. 1–4.

[47] J. Zhou, H. Zhang, and L. Mo, "Two-dimension localization of passive RFID tags using AOA estimation," in *Proc. IEEE Int. Instrum. Meas. Technol. Conf.*, May 2011, pp. 1–5.
[48] E. H. Lockwood, "Revision course in school mathematics. By HE parr. pp. viii, 206. 97p.(bell.)," *Math. Gazette*, vol. 56, no. 397, pp. viii–242, 1972.
[49] R. Standard, "Low level reader protocol (LLRP) 2 version 1.1 3," *Nature*, vol. 18, p. 19, 2005.
[50] *EPC^{TM} Radio-Frequency Identity Protocols Class-1 Generation-2 UHF RFID—Protocol for Communications at 860 MHz–960 MHz*, IncTM, EPCGlobal, Version, 2005.
[51] L. M. Ni, Y. Liu, Y. C. Lau, and A. P. Patil, "LANDMARC: Indoor location sensing using active RFID," *Wireless Netw.*, vol. 10, no. 6, pp. 701–710, 2004.

Ge Wang received the Ph.D. degree from Xi'an Jiaotong University in 2019. She was a Visiting Student at the University of California at Santa Cruz from 2017 to 2019. She is currently an Assistant Professor at Xi'an Jiaotong University. Her research interests include wireless sensor networks, RFID, and mobile computing.

Xiaofeng Shi (Graduate Student Member, IEEE) received the bachelor's and master's degrees from the Department of Computer Science and Technology, Nanjing University, China, in 2014 and 2017, respectively. He is currently pursuing the Ph.D. degree with the Department of Computer Science and Engineering, UC Santa Cruz. His research interests include wireless sensing, computer networks, and learning augmented algorithms and systems.

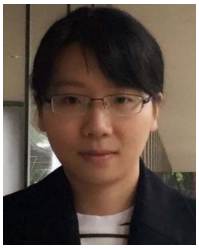

Haofan Cai received the B.Eng. degree from the Southern University of Science and Technology in 2016. She is currently pursuing the Ph.D. degree with the University of California at Santa Cruz. Her research interests include wireless sensor networks and RFID.

Chen Qian (Senior Member, IEEE) received the Ph.D. degree from The University of Texas at Austin in 2013. He is currently an Assistant Professor at the Department of Computer Engineering, University of California at Santa Cruz. His research interests include computer networking, data-center networks, software-defined networking, and mobile computing.

Han Ding received the Ph.D. degree in computer science and technology from Xi'an Jiaotong University in 2017. She is currently an Associate Professor with Xi'an Jiaotong University. Her research interests include RFID systems and smart sensing.

Wei Xi (Member, IEEE) received the Ph.D. degree in computer science and technology from Xi'an Jiaotong University in 2014. He is currently an Associate Professor with Xi'an Jiaotong University. His research interests include wireless networks, smart sensing, and mobile computing. He is a member of CCF and ACM.

Kun Zhao (Member, IEEE) received the Ph.D. degree in computer science from Xi'an Jiaotong University in 2019. He is currently an Assistant Professor with the School of Computer Science and Technology, Xi'an Jiaotong University. His main research interests include wireless networks, smart sensing, and federated learning. He is a member of ACM.

Jizhong Zhao (Member, IEEE) received the Ph.D. degree in computer science and technology from Xi'an Jiaotong University in 2001. His research interests include computer software, pervasive computing, distributed systems, and network security. He is a member of CCF and ACM.

Jinsong Han (Senior Member, IEEE) received the Ph.D. degree in computer science from The Hong Kong University of Science and Technology in 2007. He is currently a Professor with Zhejiang University. His research interests include mobile computing, RFID, and wireless networks. He is a Senior Member of ACM.